DOI: 10.13009/EUCASS2023-061
Aerospace Europe Conference 2023 – 10TH EUCASS – 9TH CEAS

Sensitivity analysis of collision avoidance manoeuvre with low thrust propulsion

Camilla Colombo†, Andrea De Vittori*, Matteo Omodei*, Juan Luis Gonzalo*, Michele Maestrini*, Pierluigi Di Lizia*, Pau Gago Padreny#, Marc Torras Ribell#, Ángel Gallego Torrego#, Diego Escobar Antón#, Roberto Armellin+,*

** Politecnico di Milano, Department of Aerospace Science and Technology, Via La Masa 34, Milan, 20156, Italy*

 # GMV, Calle Isaac Newton 11, Tres Cantos, 28670, Spain

+University of Auckland, Engineering block 1 - Bldg 401, 20 Symonds St, Auckland Central, Auckland, 1010, New Zealand

camilla.colombo@polimi.it, andrea.devittori@polimi.it, matteo.omodei@mail.polimi.it, juanluis.gonzalo@polimi.it, michele.maestrini@polimi.it, pierluigi.dilizia@polimi.it, pau.gago.padreny@gmv.com marc.torras.ribell@gmv.com, agtorrego@gmv.com, descobar@gmv.com, roberto.armellin@auckland.ac.nz

† Corresponding Author

Abstract

In this paper an analytical and a semi-analytical technique to compute low thrust Collision Avoidance Manoeuvres (CAMs) are presented and tested against a large dataset of Conjunction Data Messages (CDMs). Such CDMs simulate real conjunctions and they are derived from a screening against a background Two-Line Element population in different orbit scenarios: early Geostationary transfer and insertion into GEO, GEO graveyard, Low Earth Orbit (LEO) to high-LEO transfer, and typical station keeping activities in LEO and GEO. A standard and an improved operational concept are simulated to manage the large uncertainty associated to the long-thrusting arcs present in the different orbit scenarios considered. On all these cases, the Close Approach (CA) is first analysed, in terms of miss distance, relative velocity and position on the b-plane, and the probability of collision at time of close approach. Then, the focus shifts to how CAM influences the displacement in the b-plane, expense for the manoeuvre and efficacy of it. For each of them, different Accepted Collision Probability Level (ACPL) thresholds and conjunction notification times are tested for CAM design. We analyse the convergence of the proposed methods and the capabilities to achieve the required ACPL for a given operational scenario.

1. Introduction

As the number of objects in Space increases, so does the number of Conjunction Data Messages (CDMs) for potential Close Approach (CA) events. Consequently, one of the pillars of space traffic management requires deriving operational concepts suitable for collision avoidance operations in low-thrust missions.
The ELECTROCAM project, funded by ESA and carried out by GMV, Politecnico di Milano and Universidad Carlos III de Madrid, has the objective of advancing the state of the art in two main aspects of low-thrust collision avoidance activities: conjunction screening under different sources of uncertainty, including those of the thruster, uncertainty propagation models [1][2], and low-thrust Collision Avoidance Manoeuvre (CAM) design and execution. Furthermore, operational constraints must also be considered in CAM design and decision-making. To meet these goals, suitable concepts are identified for each of the different scenarios where low thrust is used, including ballistic, disposal and orbit-raising scenarios, and tested against a large conjunction dataset. As part of this analysis, we developed different analytical and semi-analytical manoeuvre optimisation methods tailored to each proposed scenario and the preliminary computation of the optimal CAM employing a low-thrust engine. Moreover, these models also enable the efficient execution of sensitivity analyses on different key parameters of CAs and CAMs. The CAM models proposed within ELECTROCAM fall into different categories, both in terms of the techniques used and their potential applications. On the one hand, an optimal control approach is followed to develop analytical Energy-Optimal CAM models, as well as semi-analytical fuel-optimal CAM design approaches that leverage the EO CAM solution as initial guess. These models consider both the Chan method for Probability of Collision (PoC) computation, as well as a more complex Gaussian Mixture Model approach. On the other hand, an analytical CAM model based on the single averaging of the equations of motion in Keplerian elements is introduced [3][4][5]. This model focuses on obtaining a computationally

DOI: 10.13009/EUCASS2023-061

efficient evaluation of the effects from a CAM, rather than on the optimization of the CAM itself, although semi-analytical optimization approaches can be built on top of it in combination with iterative numerical methods. Finally, aside from these analytical and semi-analytical methods, fully numerical approaches have also been developed within the project.

In this paper, the proposed analytical fuel-optimal CAM technique is briefly described, and some application cases are shown. A large dataset of CDMs is created, simulating real conjunctions. These are derived from a screening against a background TLE population in different orbit scenarios: early Geostationary transfer and insertion into GEO, GEO graveyard, Low Earth orbit (LEO) to high-LEO transfer, and typical station keeping activities in LEO (Starlink's orbit) and GEO. Covariance information of the secondary is derived from statistical analysis on CSpOC CDMs for ESA missions. For the primary, improved operational concepts are simulated to manage the large uncertainty associated to the long-thrusting arcs present in the different orbit scenarios considered. This way, the predicted state better matches the flown trajectory, and the covariance growth is kept within limits reasonable for an accurate risk analysis. These concepts are compared against current or nominal operational concepts.
On all these cases the CA is first analysed, in terms of miss distance, relative velocity and position on the b-plane, and the probability of collision at Time of Close Approach (TCA). Then, the focus shifts to how the CAM influences the displacement in the b-plane, expense for the manoeuvre and efficacy of it. For each of them, different Accepted Collision Probability Level (ACPL) thresholds and conjunction notification times are tested for CAM design. We analyse the convergence of the proposed methods and the capabilities to achieve the required ACPL for a given operational scenario. In case the required ACPL cannot be fulfilled, due to a short warning time, a minimisation of the probability of collision is ensured through a semi-analytical solution.

2. Fundamentals

This section provides a brief overview of the mathematical framework to develop the semi-analytical fuel-optimal CAM policies for both tangential, radial firings and a simple switch-off strategy over a given thrust profile in Electric Orbit Raising (EOR) cases.

2.1 B-plane definition and Chan's PoC

Bombardelli in [6] describes the b-plane derivation, a framework widely adopted in the literature for short-term encounters. In this coordinate system, the collision probability can be made equivalent to integrating a properly scaled isotropic Gaussian distribution function over an elliptical cross-section. If the latter is approximated as a circular cross-section of equal area, the final computation of the collision probability reduces to a Rician integral that can be computed with the convergent series found by Chan [7]:

$$PoC = e^{-\frac{v}{2}} \sum_{m=0}^{\infty} \frac{v^m}{2^m m!} \left[1 - e^{-\frac{u}{2}} \sum_{k=0}^{m} \frac{u^k}{2^k k!} \right] \tag{1}$$

where u is the ratio of the impact cross-sectional area to the area of the 1σ covariance ellipse in the b-plane, and v is the Squared Mahalanobis Distance (SMD) between the operative satellite and the piece of debris:

$$u = \frac{R_A^2}{\sigma_\xi \sigma_\zeta \sqrt{1 - {\rho_{\xi\zeta}}^2}}, \qquad v = \left[\left[\left(\frac{\xi_e}{\sigma_\xi} \right)^2 + \left(\frac{\zeta_e}{\sigma_\zeta} \right)^2 - 2{\rho_{\xi\zeta}}^2 \frac{\xi_e}{\sigma_\xi} \frac{\zeta_e}{\sigma_\zeta} \right] \right] / \left(1 - {\rho_{\xi\zeta}}^2 \right) \tag{2}$$

2.2 Analytical Energy Optimal CAM design

The energy-optimal formulation takes inspiration from [8]. Within the ELECTROCAM project, if the primary spacecraft (i.e., the manoeuvrable one) features a low-thrust propulsion system, CAM is assumed to orient the thruster along the tangential direction for advanced CAM notification or radial direction for just-in-time manoeuvres. The energy-optimal acceleration profile serves to guess firing windows for fuel-optimal adaptations. Let us delve into the controlled motion of the primary around the Earth, considering the propelled Keplerian dynamics introduced and experiencing a conjunction event with a secondary object. Chan-based CAMs are stated as an indirect Energy Optimal Control Problem (EOCP):

DOI: 10.13009/EUCASS2023-061

$$\min J(\boldsymbol{a}_c) = \gamma\psi\big(\boldsymbol{r}(t_f), t_f\big) + \int_{t_0}^{t_f} \left\{\frac{1}{2}{a_c}^2 + \boldsymbol{\lambda}^{\mathrm{T}}(t)[\boldsymbol{x}(t) - f(\boldsymbol{x}, \boldsymbol{a}_c)]\right\} dt \tag{3}$$

where:

$$\psi\big(\boldsymbol{r}(t_f), t_f\big) = d_M^2\big(r_f\big) - \overline{d_M^2} = 0 \tag{4}$$

In Eq. (4), $d_M^2\big(r_f\big)$ is the actual SMD, and d_M^2 is the target value linked to a desired Chan's PoC. The resulting Euler-Lagrange equations for tangential manoeuvres are:

$$\tilde{\boldsymbol{f}} = \begin{cases} \dot{\boldsymbol{r}} = \boldsymbol{v} \\ \dot{\boldsymbol{v}} = -\dfrac{\mu}{r^3}\boldsymbol{r} - \Big(\boldsymbol{\lambda}_v \cdot \dfrac{\boldsymbol{v}}{v}\Big)\dfrac{\boldsymbol{v}}{v} \\ \dot{\boldsymbol{\lambda}}_{r=} - \dfrac{\mu}{r^3}\boldsymbol{\lambda}_v - \dfrac{3\mu\boldsymbol{r}\cdot\boldsymbol{\lambda}_v}{r^3}r \\ \dot{\boldsymbol{\lambda}}_v = -\lambda_r + 2\left(-\left(\dfrac{\boldsymbol{\lambda}_v\cdot\boldsymbol{v}}{v^2}\right)^2\boldsymbol{v} + \left(\dfrac{\boldsymbol{\lambda}_v\cdot\boldsymbol{v}}{v^2}\right)\boldsymbol{\lambda}_v\right) \end{cases}$$

$$BC: \begin{cases} \boldsymbol{r}(t_0) = \boldsymbol{r}_0 \\ \boldsymbol{v}(t_0) = \boldsymbol{v}_0 \\ \boldsymbol{\lambda}_r\big(t_f\big) = \nu\dfrac{\partial d_M^2\big(\boldsymbol{r}_f\big)}{\partial \boldsymbol{r}_f} = 2\nu\boldsymbol{R}_{2D}^T\boldsymbol{C}^{-1}\boldsymbol{R}_{2D}\big(\boldsymbol{r}_f - \boldsymbol{r}_s\big) \\ \boldsymbol{\lambda}_v\big(t_f\big) = \nu\dfrac{\partial d_M^2\big(\boldsymbol{v}_f\big)}{\partial \boldsymbol{v}_f} = 0 \\ \phi\big(\boldsymbol{r}(t_f), t_f\big) = 0 \end{cases} \tag{5}$$

$\boldsymbol{r}_f$ and $\boldsymbol{r}_s$ are the primary's position at TCA on the controlled manoeuvre and the position associated with the secondary object. The goal is to retrieve the initial costates $\boldsymbol{\lambda}_{r0}$, $\boldsymbol{\lambda}_{v0}$ by analytically reducing the Two-Point Boundary Value Problem (TPBVP) into an Initial Value Problem (IVP) thanks to motion linearization. A thorough explanation of the solution scheme is given in [8]. Turning to radial manoeuvres, the Euler-Lagrange equations are similarly derived by following the same steps of the tangential counterpart.

2.3 Asymptotic solution of the two-body problem with tangential acceleration

Bombardelli et al. derived in [9] an analytical solution to the two-body problem perturbed by a constant tangential acceleration with the aid of perturbation theory. If all acting forces have a zero component along the normal direction to the orbital plane and if it undergoes a tangential acceleration a_t such that:

$$\epsilon = \frac{a_t}{\mu/r_0^2} \ll 1 \tag{6}$$

it possible to express the approximated evolution of the three generalized orbital parameters q_1, q_2 and q_3 and the time t as functions of a new variable $\tilde{E}$ as:

$$q_j\left(\tilde{E}, \epsilon\right) = q_{j0}\big(\tilde{E}\big) + \epsilon q_{j1}\big(\tilde{E}\big) + o(\epsilon), \quad t\big(\tilde{E}, \epsilon\big) = t_0\big(\tilde{E}\big) + \epsilon t_1\big(\tilde{E}\big) + o(\epsilon) \tag{7}$$

j spans from 1 to 3 and the analytical expressions of $q_{j0}\big(\tilde{E}\big)$, $q_{j1}\big(\tilde{E}\big)$, $t_0\big(\tilde{E}\big)$, and $t_1\big(\tilde{E}\big)$ are available in [9]. The analytical propagator, given $\tilde{E}$, an initial state $\boldsymbol{x}_{p0}$ and ϵ outputs the time of flight and the ECI state $\boldsymbol{x}_{pf}$ at that $\tilde{E}$. This formulation comes in handy for fuel-optimal tangential CAMs detailed in Sec. 3.1.

2.4 Differential Algebra

The Differential Algebra (DA) is a tool that allows the efficient expansion of sufficiently often differentiable functions as Taylor polynomials in a computer environment [10]. In short, a function f can be represented by its Taylor expansion

DOI: 10.13009/EUCASS2023-061

around an expansion point truncated at an arbitrary finite order n^{DA} so that it can be manipulated and evaluated by means of simple arithmetic expressions.

2.5 Picard-Lindelöf iteration

In the context of proving the uniqueness of an IVP solution, Emile Picard and Ernst Lindelöf formulated a method based on successive approximations. Thus, given the IVP:

$$\begin{cases} \dot{\boldsymbol{x}} = \boldsymbol{f}(\boldsymbol{x}(t), t) \\ \boldsymbol{x}(t_0) = \boldsymbol{x}_0 \end{cases} \tag{8}$$

the approximate solution of the IVP can be obtained by recursively solving the iteration scheme [11]:

$$\boldsymbol{x}_{k+1}(t) = \boldsymbol{x}_0 + \int_{t_0}^{t} \boldsymbol{f}(\boldsymbol{x}_k(s), s)\, ds \tag{9}$$

$k = 0,1,2\ldots n^{PL}$ with n^{PL} expressing the expansion order. This kind of iterative procedure combined with differential algebra is leveraged in Sec. 3.2 to represent radial propelled manoeuvres.

3. Semi-analytical Fuel-optimal tangential and radial CAMs with Chan's PoC boundary condition

This section describes lightweight algorithms to perform a bang-bang CAM adaptation with just one firing window. As reported in Sec 2.1, the energy-optimal Chan CAM is brought up because it suggests possible fuel-optimal firing windows nearby the local acceleration norm maxima. At first, the equivalent burning time t_b is estimated using the energy-optimal acceleration resulting from the tangential or radial continuous thrust:

$$t_b = \frac{\Delta v}{a_{max}} = \frac{1}{a_{max}} \int_{t_0}^{t_f} a_{EOCP}(t)\ dt \tag{10}$$

where a_{max} is the engine acceleration level. Then, the idea is to define a threshold acceleration ($a_{c,th}$) so that the thrusters are fired up for $a_{EOCP} > a_{c,th}$ and switched off otherwise. To this purpose, once a_{max} is set, a bisection-like method retrieves $a_{c,th}$ and the corresponding switch on/off time instants (see Figure 1):

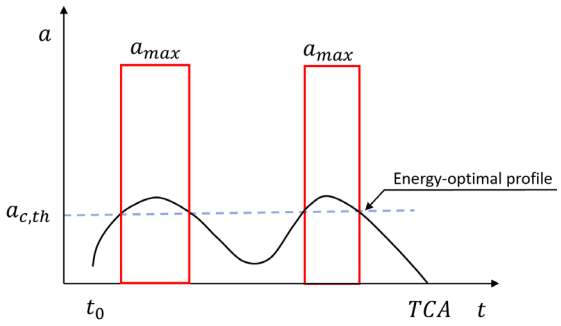

Figure 1: Selection of candidate firing windows through a bisection like procedure.

It is vital, before moving forward, to point out that in the shortlisted window, the energy-optimal solution is aligned or anti-aligned with enforced thrust direction. a_{max} sign should be adjusted coherently with this reasoning.

3.1 Tangential Fuel-Optimal CAMs

For tangential manoeuvres, being cost-effective for advanced CAM notification, there may be more than one candidate firing window. Indeed, the bang-bang strategy plans for each candidate arc a CAM, and it outputs the one with the lowest firing time as required by this project. Up to this stage, the nominal firing windows have been sought in the

DOI: 10.13009/EUCASS2023-061

time domain. However, the envisaged semi-analytical approach is thought in the frame of generalised orbital parameters $[q_1, q_2, q_3]$ particularised by C. Bombardelli that a are function of the true anomaly θ (for further details please check [9]). It should be mentioned that the Keplerian parameters continuously vary during accelerated dynamics. Consequently, shaping the thrust arc on the ballistic trajectory is a reasonable approximation from a true anomaly perspective only in the case of short firings featuring a value of a_{max} compatible with low-thrust propulsion systems. The aim is to obtain the first guess on the firing windows ($\Delta\theta_{ON}$) derived from Sec. 3 that will be expanded or shortened according to the solution process. For clarity, it is assumed to work with ON-OFF or OFF-ON-OFF acceleration profiles. With a Non-Linear Programming (NLP) formulation, the firing window updates to meet the final constraint in terms of SMD. To this end, a coefficient $\alpha > 0$ is multiplied by $\Delta\theta_{ON}$ to generate a new firing window. Usually, this kind of iterative processes demand a guess on the independent variable ($\alpha = 1$). The algorithm is extremely efficient because all the numerical propagations in the NLP problem are analytical for ballistic and thrusting arcs (see Sec. 2.3).

3.2 Radial Fuel-Optimal CAMs

The problem formalizes as a TPBVP since the satellite's initial state with the enforced SMD are known. As for the tangential counterpart, the objective is to define the duration of the firing arc that ensures the final constraint is satisfied, given the maximum acceleration a_{max} the thrusters can provide. The radial control could be more effective than the tangential one for just-in-time manoeuvres (less than 0.2/0.3 orbits before TCA). In addition, thanks to the acceleration magnitude, the bisection algorithm in Sec. 3 should exhibit only one firing window in that true anomaly range. Once the nominal firing time is available, the first step for the problem-solution is the numerical propagation of the accelerated dynamics in the nominal time window, i.e., (t_{on}, t_{off}), selected by the bisection routine. The state $\boldsymbol{x}_p(t)$ at t_{off} is known through a numerical integration of the propelled dynamics. The next step consists in initializing Differential Algebra by selecting the number of DA elements, the desired Taylor expansion order n^{DA} and the expansion points around which to compute the Taylor polynomials. In the present approach, the DA variables are the 6-dimensional state vector $\boldsymbol{x}_p(t_{off})$. Adopting DA-based Picard-Lindelöf iterations, for a desired order of expansion n^{PL} it is possible to compute the DA representation of the state $[\boldsymbol{x}_p(t_{off})]$:

$$[\boldsymbol{x}_p(t_{off})] = \left[\boldsymbol{x}_{n^{PL}}(t_{off})\right] = \boldsymbol{x}_p(t_{off}) + \int_0^{\delta t_{off}} [\boldsymbol{f}]\left(\left[\boldsymbol{x}_{n^{PL}-1}\right], s\right)\, ds \tag{11}$$

$[\boldsymbol{x}_p(t_{off})]$ is now a polynomial vector function $\boldsymbol{p}(\delta t_{off})$ just dependent on δt_{off}. Note that, as long as δt_{off} is within the convergence radius of $\boldsymbol{p}$, Eq. (11) will yield a good approximation of the state $\boldsymbol{x}_p(t)$ around t_{off}. The DA integration method appears to be quite efficient in deriving the polynomial expression. A Netwon-like zero-finding approach describes how by tuning t_{off}, and then propagating through a ballistic motion, the SMD constraint is compliant up to an arbitrary threshold at TCA. If $\delta t_{off,guess}$ is too large to faithfully represent the real dynamics, a new Picard-Lindelöf polynomial can be recomputed at the expansion point ${t_{off}}^* = t_{off} + \delta t_{off,guess}$. Recall, then, the Newton-based algorithm to assess the new ${\delta t_{off,guess}}^*$.

3.3 EOR CAMs with thruster shutdown

EOR scenarios differ greatly from the ballistic cases because the primary object has a prescribed control profile history. The EOR Chan's CAM should be then envisioned to satisfy the boundary constraint on PoC and limit the offset with respect to the mission related trajectory. To this aim, the drafted EOR Chan's CAM requires an equally spaced in time (10 s) numerical integration from the latest available OPM state up to conjunction. Following, a spline interpolation (called $\boldsymbol{p}_{spline}(t)$) in the time domain using not-a-knot end conditions fills the gaps among the integration points. The interpolated value at a query point is based on a cubic interpolation of the values at neighbouring grid points in each respective dimension. The exact switch-off time to impose a PoC limit requires a boundary function, as already seen in the preceding methods. Once the boundary function is set, a bisection-like method retrieves the switch-off time t_{off}. The algorithm at a generic iteration evaluates $\boldsymbol{p}_{spline}(t)$ at t_{off}. From t_{off} to TCA it leverages an analytical ballistic propagation.

DOI: 10.13009/EUCASS2023-061

4. Approach for conjunction screening and risk analysis

This section describes the simulation setup for conjunction screening, which is then followed by an approach for CAMs. A summary of the steps in the simulation is presented in Figure 2.

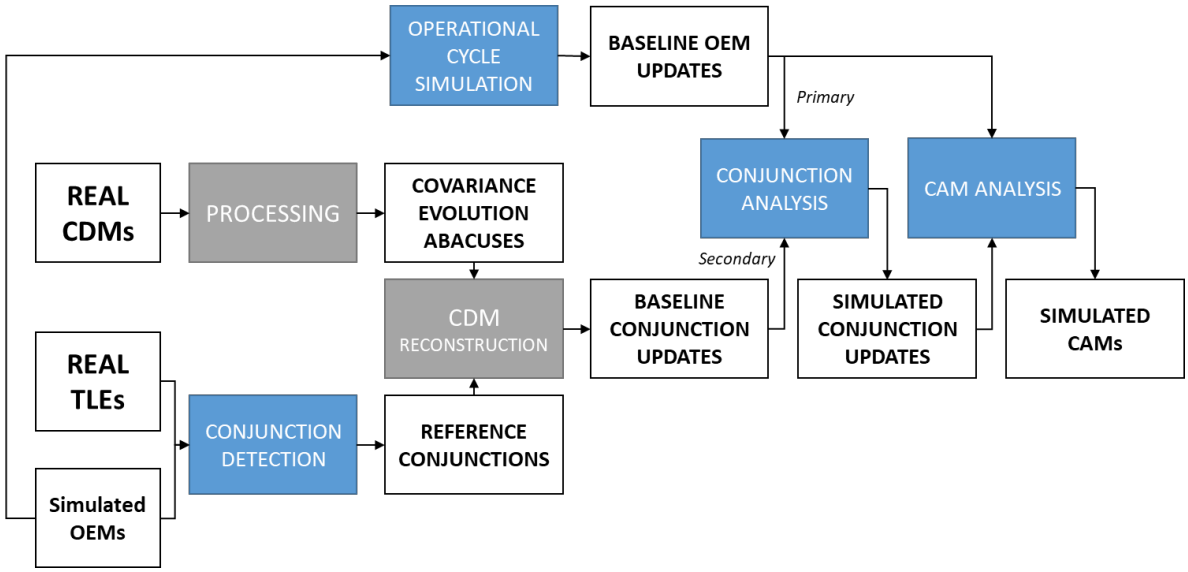

Figure 2: Conjunction screening and risk analysis workflow.

The main steps are introduced below:

- Real CDMs are processed to obtain covariance evolution abacuses for the background population.
- Real TLEs from different days and simulated OEMs for the primary objects are used to detect conjunctions, which are taken as the reference (real) geometry.
- CDM updates before TCA are reconstructed based on the covariance abacuses and the reference conjunctions.
- Baseline OEMs for the primary objects are generated based on the simulation of the operational cycle, including sensor tracking, orbit determination (OD) and propagation (which involves propagation of a thrusting arc and its associated error for continuous thrusting scenarios). These OEMs differ from the simulated OEMs. The difference is due to the simulation of the operational cycle.
- A conjunction analysis is performed to assess the risk of the baseline conjunction updates, updating all conjunction parameters (i.e., TCA, PoC, geometry…)
- For the simulated conjunction updates that achieve ALERT risk level, a CAM is computed.
- The conjunction screening includes conjunction detection and conjunction risk analysis. For these simulations, it has been found to be suitable to define these as two different processing steps. The first one is intended to create the conjunction events while the second one is intended to simulate the event evolution through the sequential CDM updates and compute the estimated risk in each update.

4.1 Reference conjunctions

In this first step, the reference conjunction events are generated based on the reference ephemeris for the primary (OEM) screened against successive TLEs for different days (i.e., against each TLE of 1-year full catalogue). The goal is to obtain a number and distribution of conjunctions (e.g., per year) which is representative of a real-life scenario. Hence, several screenings might be needed against different catalogue epochs and/or different catalogues to have a statistical meaningful set of conjunctions.
To simplify the simulations, a given time window fixed in time (e.g., one full day) is considered. Then, a single primary OEM (reference scenario trajectory) is screened against successive TLEs. Because the goal of these simulations is to have statistical results, rather than particular results for a specific mission and time window, the TLE catalogue of successive days can be modified, changing the epoch of the TLEs to match the analysis time window (e.g., 2010/01/08). This will create a new space object catalogue which is different from day to day. This is particularly useful for objects which have an orbital period different than a day. For GEO, different permutations of the background catalogue are required, and detailed next.

DOI: 10.13009/EUCASS2023-061

To increase the amount of data for the posterior statistical analysis, the number of background TLE catalogues can be increased by modifying the epoch of the TLEs in each run by a different amount of time (i.e. n hours). This simulates different catalogues which are representative of the real one.
The screenings are run for a time span of 1 day, after a propagation of 7 days in LEO and 15 in GEO. This is only to detect the real conjunction geometry. The updates of the events will be generated afterwards. Hence, the orbits of the primary from the OEMs and the TLEs are considered "perfect" in this stage of the simulation.
The use of very large screening volumes is needed to assure the detection of all relevant events.
This first stage does not incorporate covariances for the primary or the secondary into the analysis because the goal is only to define the real geometry of the conjunctions for events that are detected.
The output of this analysis is the list of conjunctions and the CDMs of the events detected with the real geometry at TCA.

4.2 Events simulations

The next step in the analysis is to compute the event evolution over time and generate updates with realistic covariances and errors in the SV estimation. In this step, the primary object is handled in a different way than the secondary objects. For the primary object, the reference ephemeris used for the screening in the previous step of the analysis is used to generate synthetic tracking for the selected sensors (e.g., GNSS, Ranging stations, …). Then an OD is performed to simulate the orbit estimate available at each time before TCA, using data only from previous epochs. Then the orbit is propagated to generate the predicted ephemeris and the covariance evolution for each update. During this process, the planned manoeuvres, for either EOR or SK, are considered.
A critical point here is the thrust error model and noise level to be used in this simulation. This needs to be further discussed. For relatively short manoeuvres (e.g., SK) a constant error model might be used, as there is little time for a meaningful time-correlation effect. For very long manoeuvres (e.g., EOR) the thrust error time correlation can have a noticeable impact on the uncertainty. In addition, if the uncertainty grows too large a non-linear propagation might be required. Nevertheless, for the short propagations used in the analysis and configuring a slightly smaller error in the thrust, linear propagation may be used.
This approach is valid to estimate the typical uncertainty evolution for each of the scenarios. However, one needs to account for several SV propagations to properly cover a realistic wide enough number of cases (i.e., some days your prediction of the thrust profile will be better than others, this is, the execution of the thrust profile will be closer or further to the planned one). This can be done with a statistical analysis generating several ephemerides with different initial positions and thrust execution error, e.g., if the thrust module has a 1-sigma of 1%, the error in the execution of the thrust profile (i.e., the discrepancy between the planned and executed) will be a random value from a gaussian distribution with a 1-sigma of 1%. Hence, a large enough number of samples has to be simulated to properly account for the statistical behaviour. The implementation and results will depend on the thrust error modelling.
For the secondary object, a prior analysis of real CDMs from Space Track is needed in order to have a statistical model (covariance abacus) of the behaviour of the SV predictions and uncertainties. Then, this data is used to simulate real event updates based on the reference conjunctions.
Table 1 show, for each scenario, an overview of the results of the TLE screening, and the considerations that have been used to obtain the results.

Table 1: Simulations information per scenario with and without operational concept

Scenario	**Concept**	**Decision to TCA [h]**	**Analysis date [day]**	**CAM type**	**ACPL limit**	**Years simulated**
LEO2LEO1	NOMINAL	12	08/01/2010	Thruster shutdown	1E-03	54.76
LEO2LEO1	IMPROVED	1	08/01/2010	Thruster shutdown	1E-04	82.14
GTO2GEO1	NOMINAL	36	02/01/2010	Thruster shutdown	1E-03	164
GTO2GEO1	IMPROVED	7	02/01/2010	Thruster shutdown	1E-04	329
LEOMEGCONST_LOW (BALLISTIC)	NOMINAL	12	09/08/2021	Acc = 0.1 mm/s2	1E-02	28.75

DOI: 10.13009/EUCASS2023-061

LEOMEGCONST_LOW (BALLISTIC)	IMPROVED	1	09/08/2021	Acc = 0.1 mm/s2	1E-02	28.75
GEOSK	NOMINAL	36	13/08/2021	Acc = 0.1 mm/s2	1E-03	65264
GEOSK	IMPROVED	7	13/08/2021	Acc = 0.1 mm/s2	1E-04	82023
GRAVEYARD	NOMINAL	36	01/01/2010	Thruster shutdown	1E-03	10917
GRAVEYARD	IMPROVED	7	01/01/2010	Thruster shutdown	1E-02	10916
GTO2GEO3	NOMINAL	36	14/06/2010	Thruster shutdown	1E-04	21352
GTO2GEO3	IMPROVED	7	14/06/2010	Thruster shutdown	1E-04	28354

5. Sensitivity analysis on the CDM scenarios

A massive set of CDM cases were generated for different orbit scenarios in Geostationary orbit station keeping (GEOSK), graveyard orbit (GRAVEYARD), GTO to GEO transfer (GTO2GEO1 and GTO2GEO3), LEO to LEO transfers (LEO2LEO) and LEO large-constellation transfers (LEOMEGCONST). For each of them two concepts of operations were considered, the STANDARD one (NO) and the new PROPOSED one (YES). The CDM cases were characterised in terms of the miss distance at TCA, the relative velocity at TCA, the PoC and the representation of the relative position vector on the b-plane at TCA. Different families can be identified corresponding to the CDM concerning the same secondary object.

5.1 CAM for the ballistic CDM scenarios

For the cases Geostationary orbit station keeping (GEOSK) we can note that, as expected, the miss distance increases in general for the cases where CAM is performed, and the effect is more visible for lower ACPL. Almost all the cases achieve convergence, indeed as visible in Figure 3a and b the required ACPL of 1e-7 (cyan), 1e-5 (magenta) and 1e-3 or 1e-4 (green) is achieved in all cases. In a few cases the threshold is not met due to numerical errors in the convergence process or due to short CAM notice as an exact ACPL is requested. The approach could be modified to minimise the PoC in case an exact ACPL is not achieved. Figure 3c and d show the projection of the CA on the b-plane. We can see how the effect of the CAM generally enlarges the b-plane coordinate with respect to the no-CAM scenario and this is visible in the b-plane time coordinate. The required Δv is in the order of 0.1 m/s for almost all the cases. Figure 3e and f show the CAM in terms of Δv. In all figures, the points in the graphs are color-coded based on the ACPL for which the CAM is performed and are compared to the nominal cases (blue).

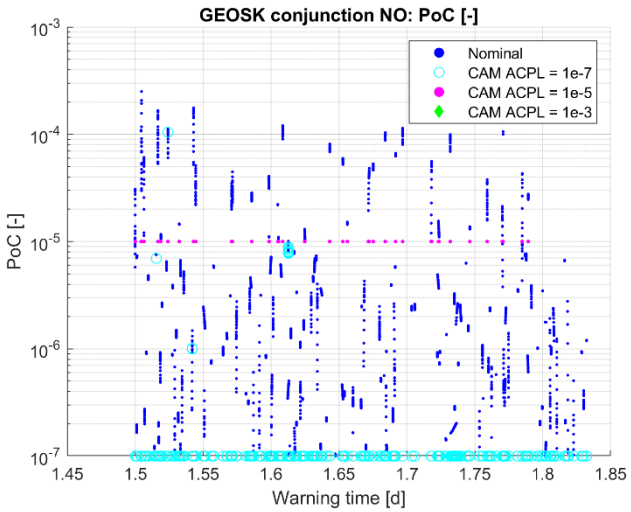

a) PoC. Concept of operations: standard

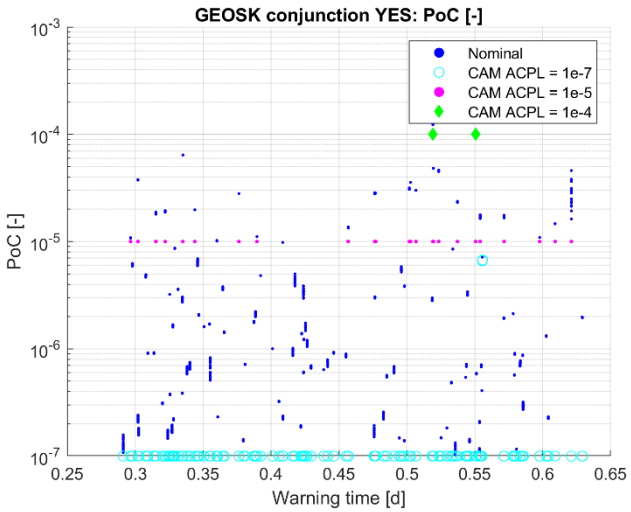

b) PoC. Concept of operations: new

DOI: 10.13009/EUCASS2023-061

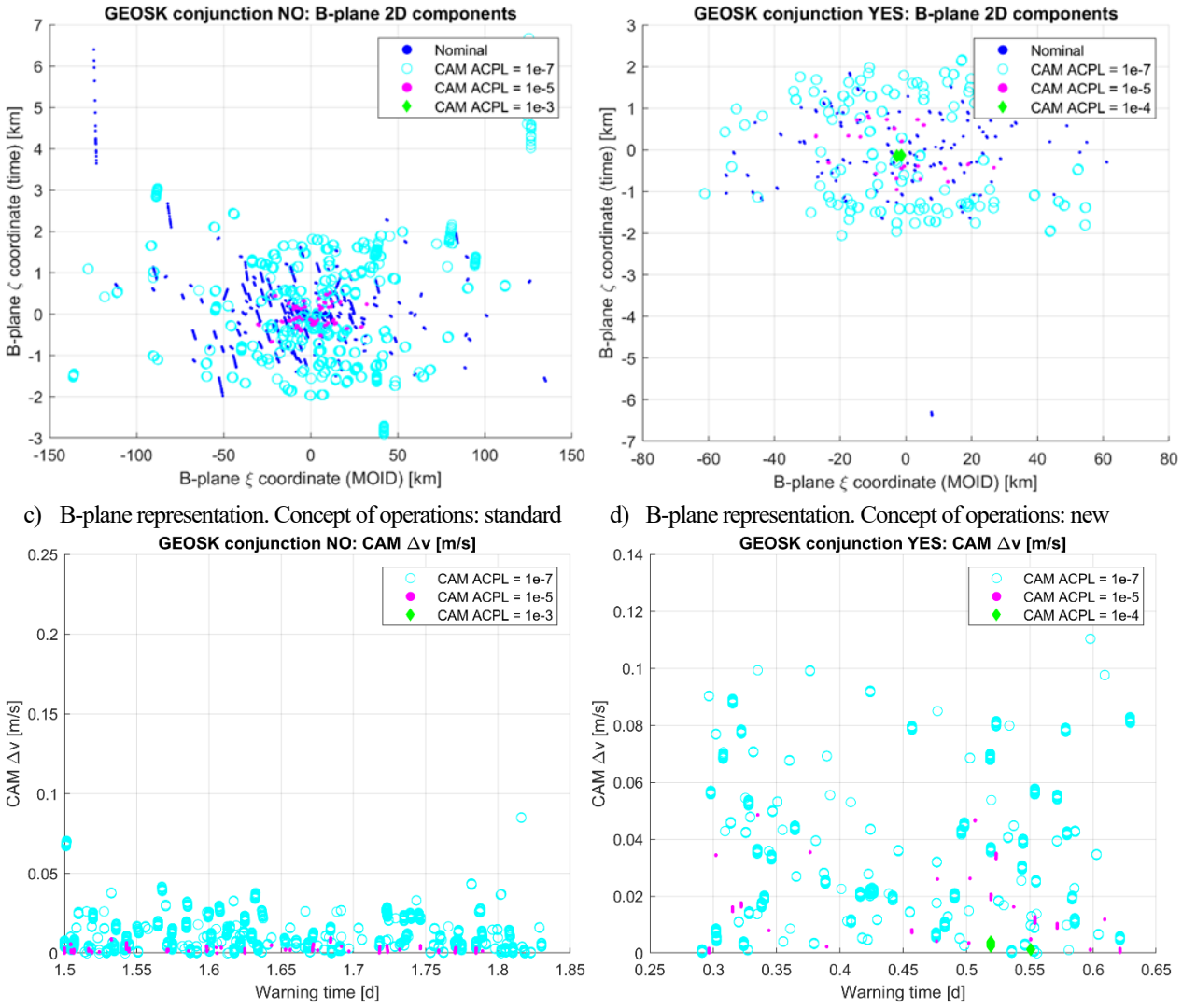

c) B-plane representation. Concept of operations: standard

d) B-plane representation. Concept of operations: new

e) CAM manoeuvre. Concept of operations: standard

f) CAM manoeuvre. Concept of operations: new

Figure 3: Characterisation of the GEOSK CAM scenarios.

To better characterise the CAM with respect to the orbit parameters Figure 4 shows for the standard and the new operational concept: the true latitude of the thrusting arc, the delta true anomaly between the engine switch-off and the CA, the delta time from switch-off until TCA and the warning time. The thrusting arc is always very short for both operational scenarios (Figure 4a and Figure 4b). For the standard operational concepts, most of the CAM solutions are clustered at full number of revolutions plus half period (Figure 4c and Figure 4e), due to the sufficient warning time (Figure 4g) to exploit the best manoeuvre location. This is because the short periodic behaviour associated to the orbital period has a relevant contribution compared to the secular due to the small number of revolutions and this contribution is maximised for half-period lead times. In the new operational concept scenario, instead, as the warning time is lower (see Figure 4h), the solutions are not clustered and performed as early as possible (Figure 4d and Figure 4f).

DOI: 10.13009/EUCASS2023-061

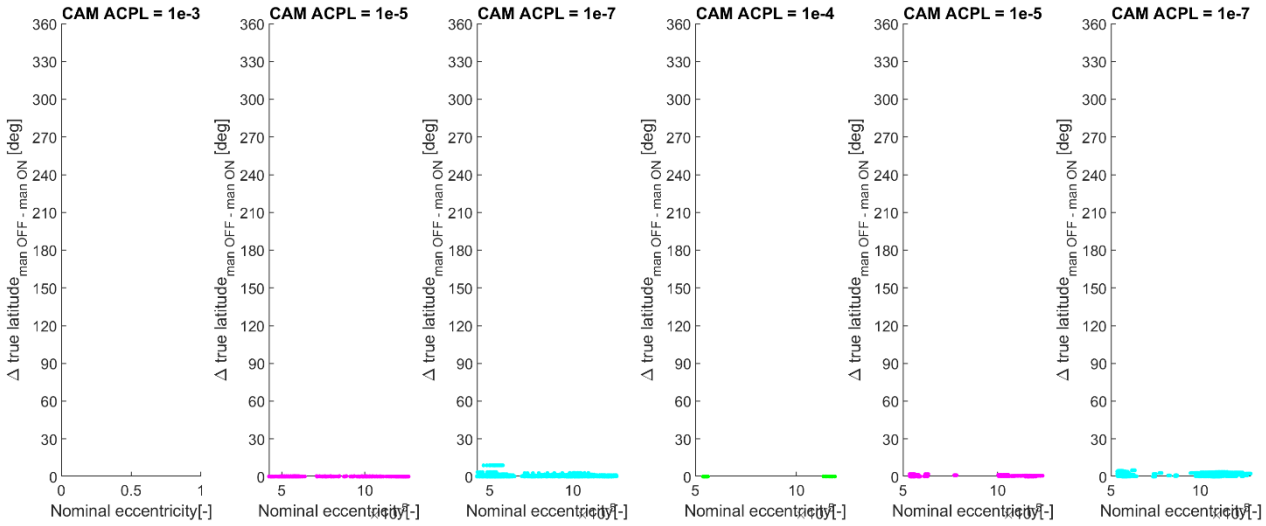

a) True latitude thrusting arc. Concept of operations: standard

b) True latitude thrusting arc. Concept of operations: new

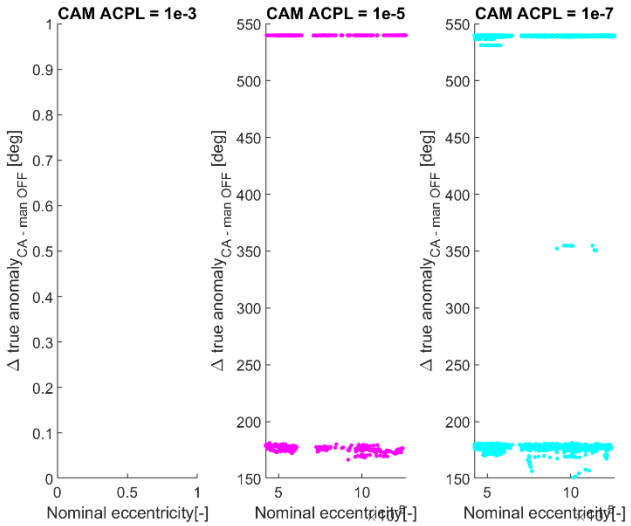

c) Delta true anomaly between the engine is turned off and the CA. Concept of operations: standard

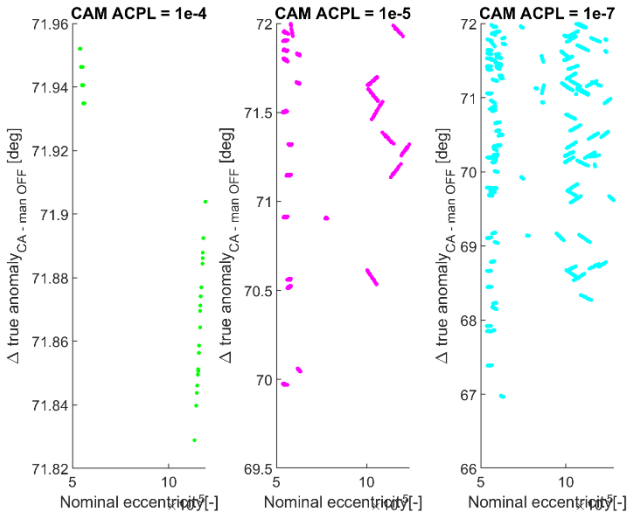

d) Delta true anomaly between the engine is turned off and the CA. Concept of operations: new

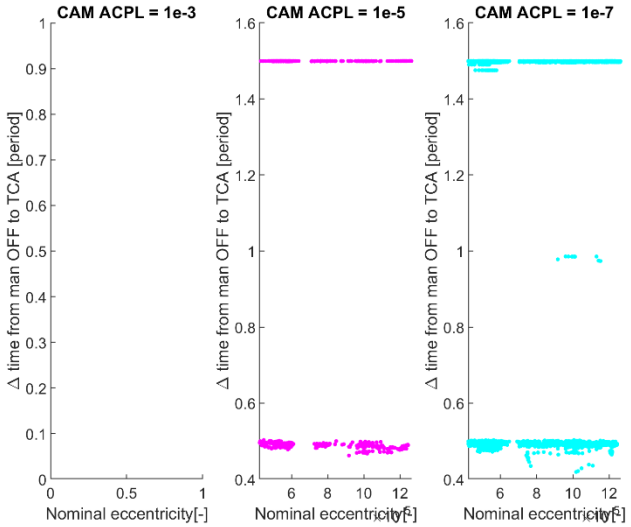

e) Delta time from manoeuvre off until TCA. Concept of operations: standard

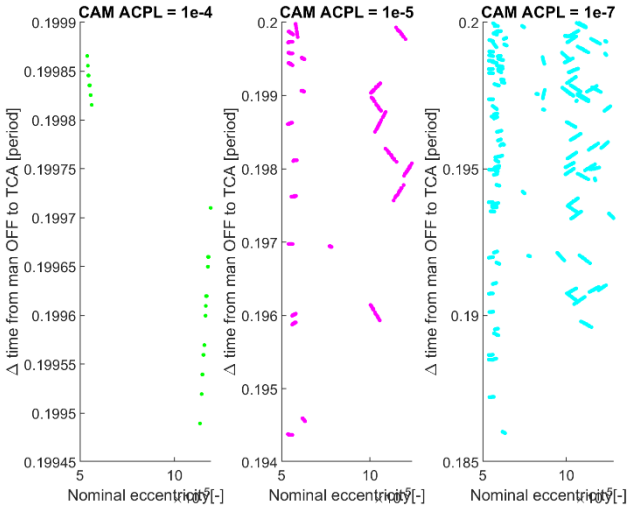

f) Delta time from manoeuvre off until TCA. Concept of operations: new

DOI: 10.13009/EUCASS2023-061

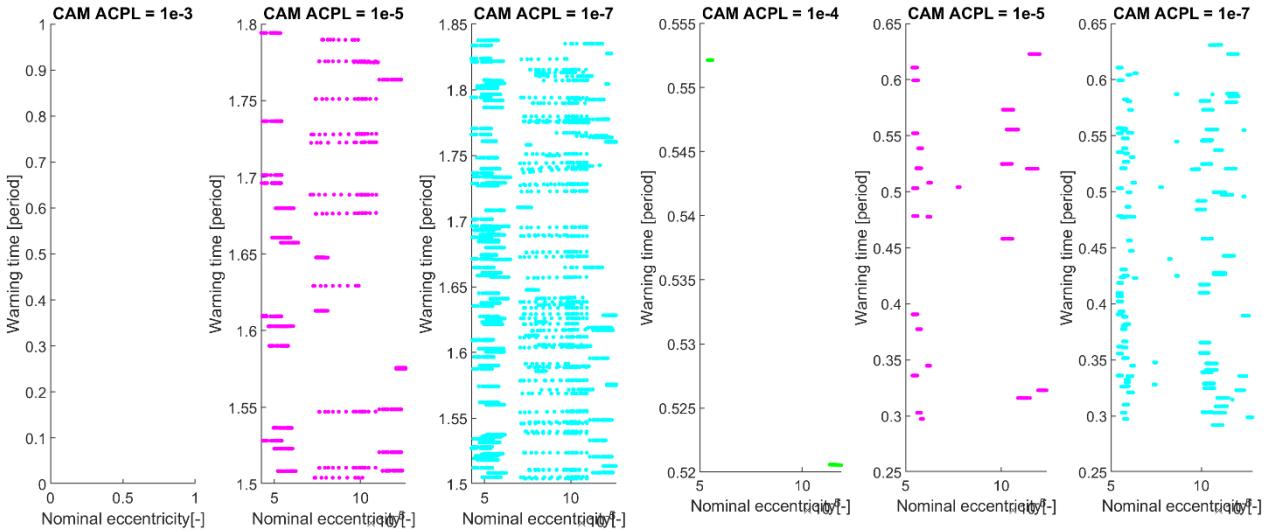

g) Warning time. Concept of operations: standard h) Warning time. Concept of operations: new

Figure 4: Characterisation of the manoeuvre versus the orbit for the GEOSK CAM scenarios.

For the cases of LEO mega-constellation transfers (LEOMEGCONST) we can note that as before for the GEOSK cases the miss distance increases in general when CAM is performed, and the effect is more visible for lower ACPL. Almost all the cases achieve convergence, indeed as visible in Figure 5a and b the required ACPL of 1e-7 (cyan), 1e-5 (magenta) and 1e-2 (green) is achieved in all cases. In a few cases of the STANDARD concept of operation scenario, the ACPL is not granted due to numerical errors in the convergence process. Instead, in the new concept of operation scenario the non-convergence is mainly related to a too short warning time and possible numerical errors in the optimization, therefore, it is not possible to always ensure the lowest ACPL of 1e-7. The approach could be modified to minimise the PoC in case an exact ACPL is not achieved. Figure 5c and d show the projection of the CA on the b-plane. We can see how the effect of the CAM generally enlarges the b-plane coordinate with respect to the no-CAM scenario. The required Δv for these cases (as visible in Figure 5e and f) is in the order of 0.7 m/s for the standard concept-of-operation scenario and ACPL of 1e-7, and is lower, as expected, for higher ACPL values. For the case of new concept-of-operation the Δv is in the order of 0.3 m/s in the case of ACPL of 1e-7 and is lower, as expected, for higher ACPL values.

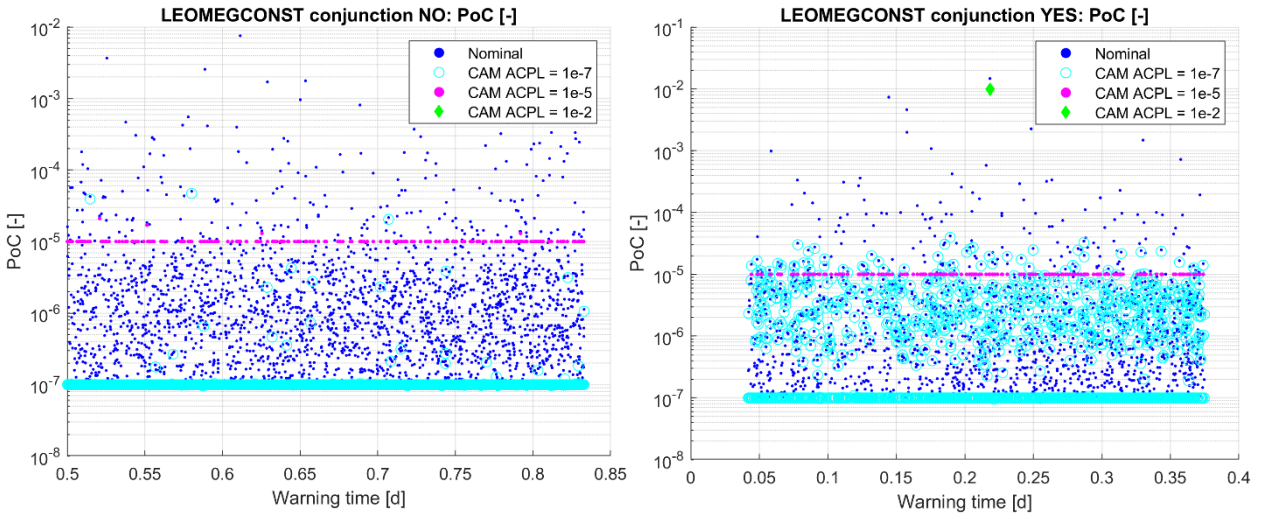

a) PoC. Concept of operations: standard b) PoC. Concept of operations: new

DOI: 10.13009/EUCASS2023-061

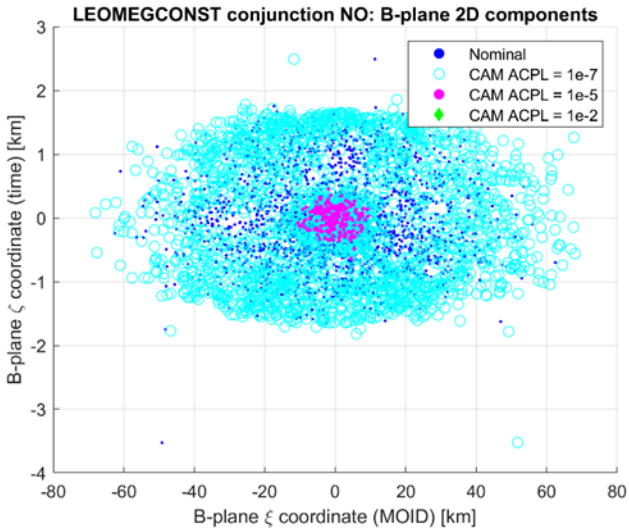

c) B-plane representation. Concept of operations: standard

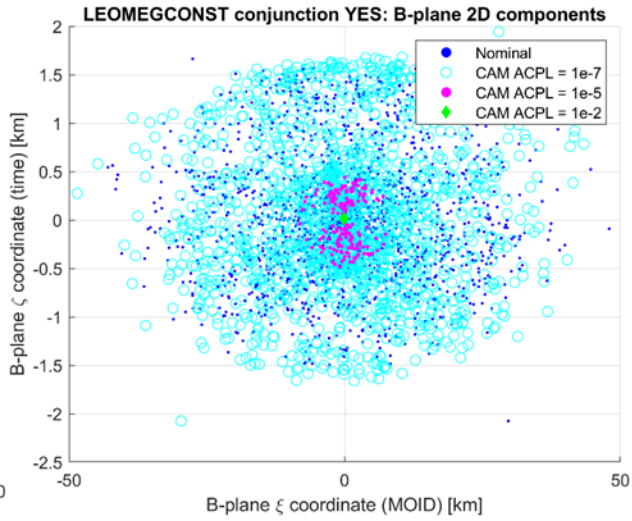

d) B-plane representation. Concept of operations: new

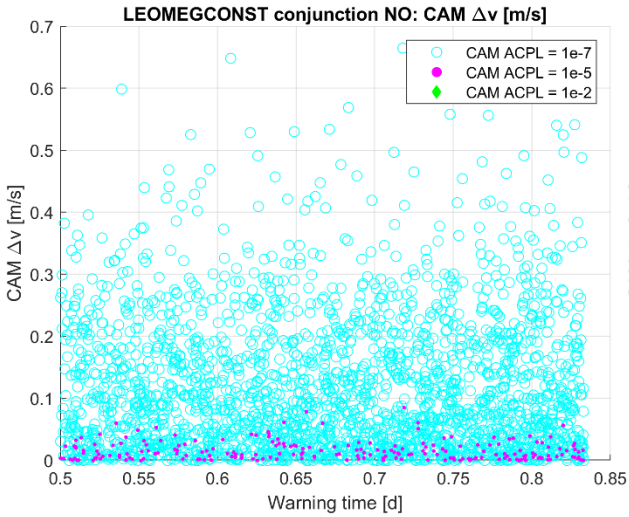

e) CAM manoeuvre. Concept of operations: standard

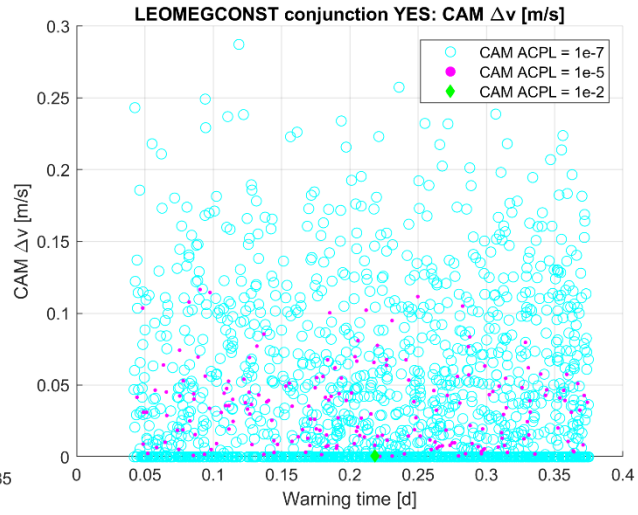

f) CAM manoeuvre. Concept of operations: new

Figure 5: Characterisation of the LEOMEGCONST CAM scenarios.

The CAM with respect to the orbit parameters is now characterised. Figure 6 shows, for the standard and the new operational concept, the true latitude of the thrusting arc, the delta true anomaly between the engine switch-off and the CA, the delta time from switch- off until TCA and the warning time. The thrusting arc can become considerably long when the required ACPL is low (Figure 6a and Figure 6b).

For the standard operational concepts, most of the solutions for CAM are clustered well in advance (see Figure 6c and Figure 6e) with some cases performed at the last half period as for those CAs a longer coasting time after manoeuvre would not improve the result. In the new operational concept scenario, instead, as the waring time is lower (see Figure 6h), the solutions are not clustered and performed as early as possible (Figure 6d and Figure 6f).

DOI: 10.13009/EUCASS2023-061

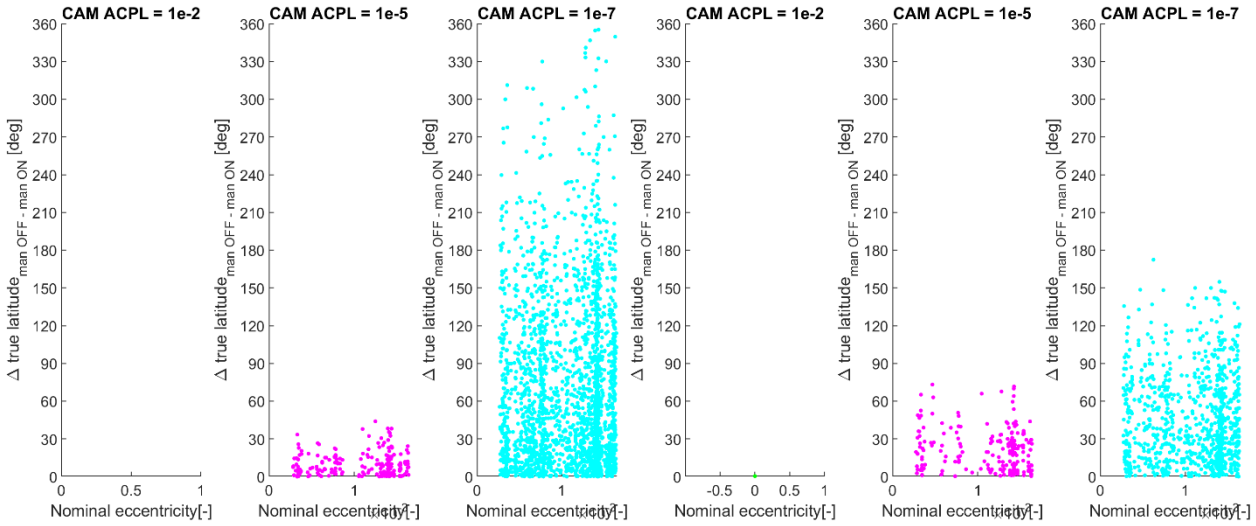

a) True latitude thrusting arc. Concept of operations: standard

b) True latitude thrusting arc. Concept of operations: new

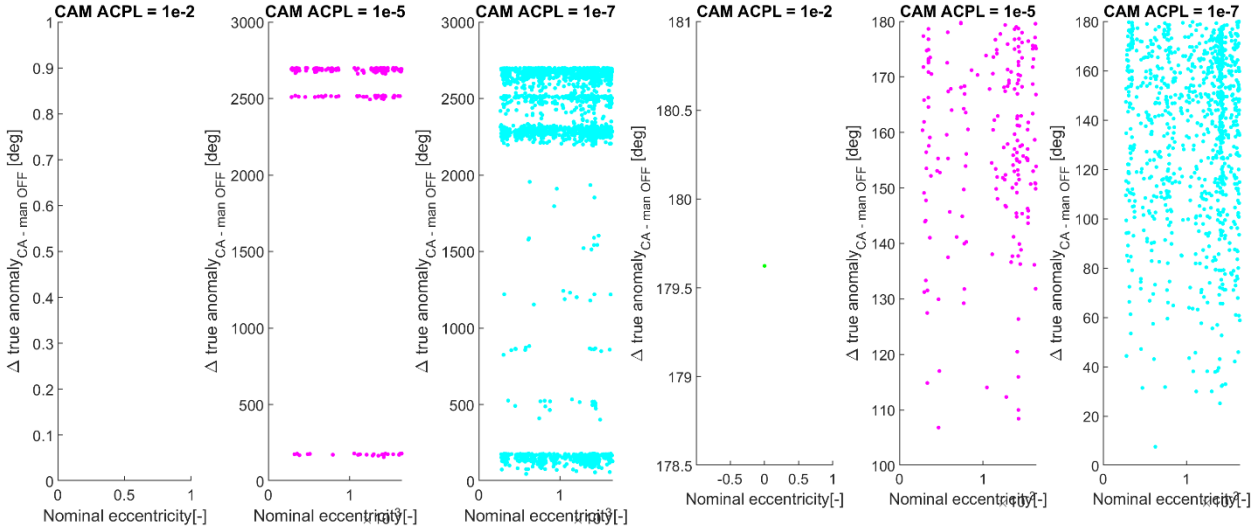

c) Delta true anomaly between the engine is turned off and the CA. Concept of operations: standard

d) Delta true anomaly between the engine is turned off and the CA. Concept of operations: new

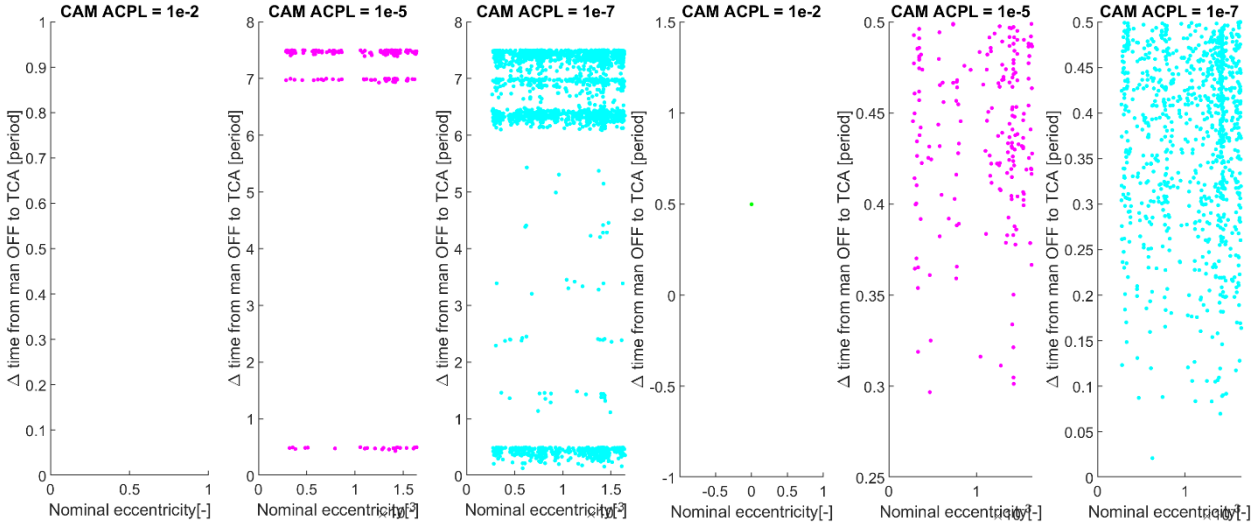

e) Delta time from manoeuvre off until TCA. Concept of operations: standard

f) Delta time from manoeuvre off until TCA. Concept of operations: new

DOI: 10.13009/EUCASS2023-061

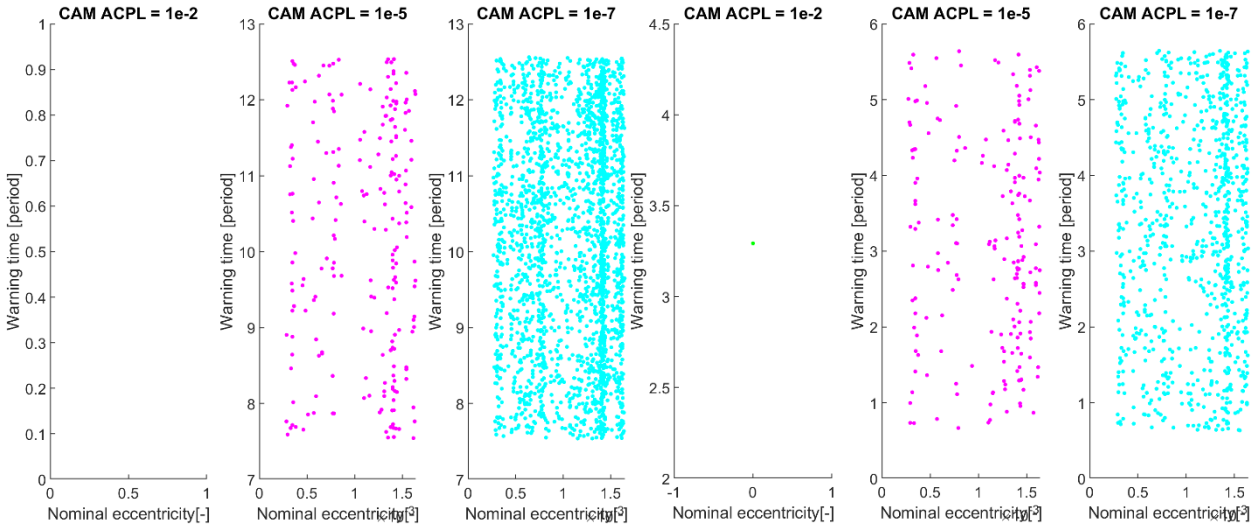

g) Warning time. Concept of operations: standard h) Warning time. Concept of operations: new

Figure 6: Characterisation of the manoeuvre versus the orbit for the LEOMEGCONST CAM scenarios.

5.2 CAM for the non-ballistic EOR CDM scenarios

Figure 7 to Figure 10 show for all the non-ballistic CDM scenarios the effect of the CAM. These are shown for the graveyard orbit (GRAVEYARD), GTO to GEO transfers (GTO2GEO1 and GTO2GEO3) and LEO to LEO transfers (LEO2LEO). In particular, the effect of the CAM was studied in terms of the miss distance at TCA, the relative velocity at TCA, the PoC, and the representation of the relative position vector on the b-plane at TCA. The points in the graphs are color-coded based on the ACPL for which the CAM is performed and are compared to the nominal cases (blue).
In this case, as the nominal scenario is non-ballistic the approach to design the manoeuvre is:

- if at TCA the PoC without manoeuvring is below ACPL then no manoeuvre is performed.
- if the PoC, by switching off the engine at decision time to TCA, is higher than the CDM PoC, then no manoeuvre is performed. The reason behind is that in just-in-time CAMs switching-off the engine may actually increase the PoC.
- if the PoC, by switching off the engine at decision time to TCA, is lower than the ACPL then a manoeuvre is planned with a bisection-like algorithm to target the required ACPL.

For the cases with EOR it was difficult to identify any regular pattern associated to the orbit geometry. This is probably due to the additional constraints in the way the CAM is performed, which does not allow to leverage the characteristics of the CA.
For the cases of graveyard orbit (GRAVEYARD) we can note that the miss distance increases in general for the cases where the manoeuvre is performed. Almost all the cases achieve convergence, indeed the required ACPL of 1e-7 (cyan), 1e-5 (magenta) and 1e-2 or 1e-3 (green) is achieved in all cases. In a few cases, the enforced ACPL is not fulfilled due to short notification time. Figure 7a and b show the projection of the CA on the b-plane. We can see how the effect of the CAM generally enlarges the b-plane coordinate with respect to the no-CAM scenario.

DOI: 10.13009/EUCASS2023-061

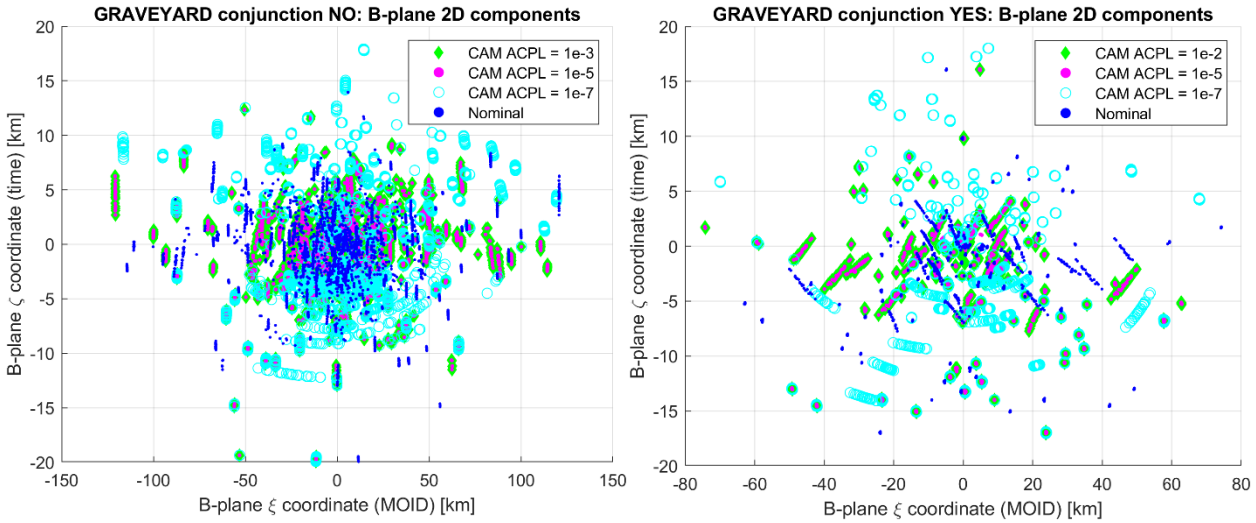

a) B-plane representation. Concept of operations: standard b) B-plane representation. Concept of operations: new

Figure 7: Characterisation of the GRAVEYARD CAM scenarios.

For the cases of GTO to GEO transfers (GTO2GEO1) shown in Figure 8 the miss distance increases in general when the manoeuvre is performed (this is only visible for the cases with ACPL of 1e-7). For the GTO to GEO case all the scenarios achieve convergence for both operational approaches, indeed the required ACPL of 1e-7 (cyan), 1e-5 (magenta), 1e3and 1e-4 (green) is achieved in all cases. Figure 8a and b show the projection of the CAM on the b-plane. We can see how the CAM generally enlarges the b-plane coordinate with respect to the no-CAM scenario.

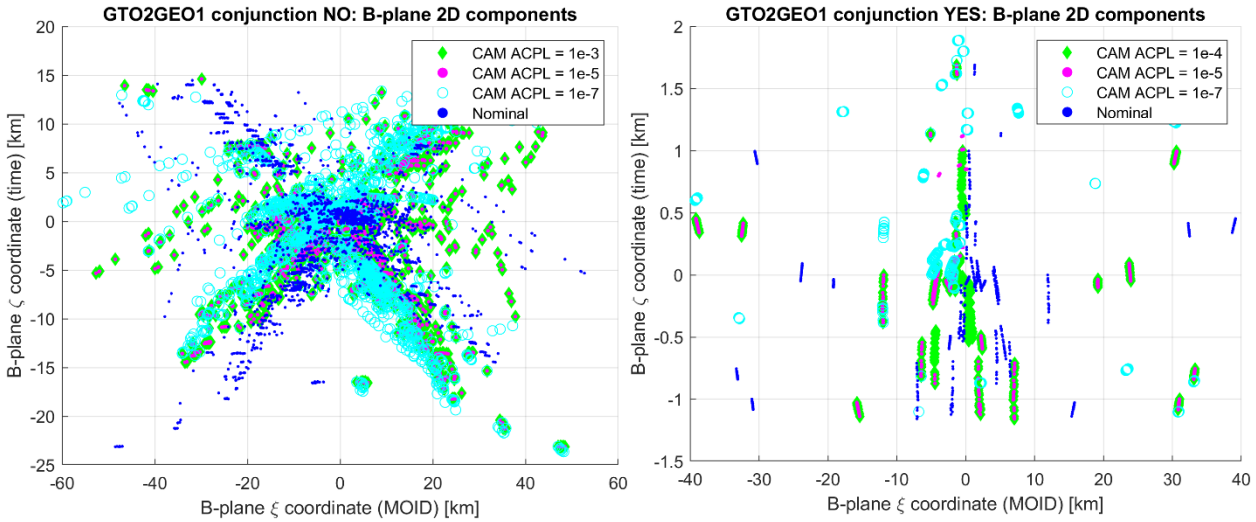

a) B-plane representation. Concept of operations: standard b) B-plane representation. Concept of operations: new

Figure 8: Characterisation of the GTO2GEO1 CAM scenarios.

For the cases of GTO to GEO transfers (GTO2GEO3) shown in Figure 9 we can note that the miss distance increases in general for the cases where the manoeuvre is performed (this is only visible for the cases with ACPL of 1e-7). All the scenarios achieve convergence, indeed the required ACPL of 1e-7 (cyan), 1e-5 (magenta) and 1e-4 (green) is achieved in all cases. Figure 9a and b show the projection of the CA on the b-plane. We can see how the effect of the CAM generally enlarges the b-plane coordinate with respect to the no-CAM scenario.

DOI: 10.13009/EUCASS2023-061

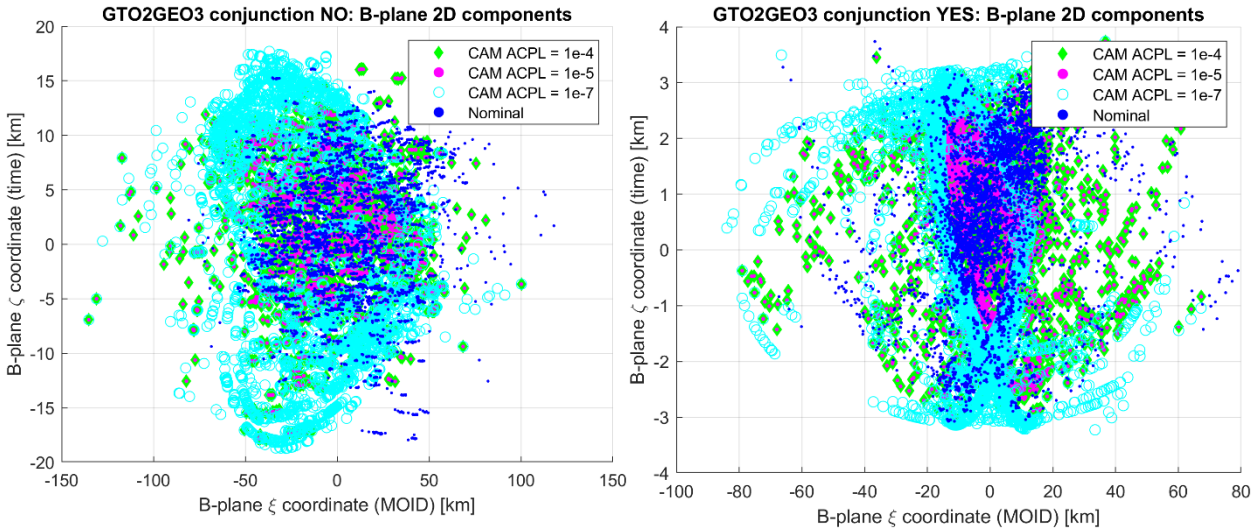

a) B-plane representation. Concept of operations: standard b) B-plane representation. Concept of operations: new

Figure 9: Characterisation of the GTO2GEO3 CAM scenarios.

Finally, for the cases of LEO to LEO transfers (LEO2LEO) shown in Figure 10 we can note that the miss distance increases in general for the cases where the manoeuvre is performed (this is only visible for the cases with ACPL of 1e-7). Almost all the cases achieve convergence indeed the required ACPL of 1e-7 (cyan), 1e-5 (magenta) and 1e-3 and 1e-4 (green) is achieved in all cases. In a few cases, the enforced ACPL is not fulfilled due to short notification time. Figure 10a and b show the projection of the CA on the b-plane. We can see how the effect of the CAM generally enlarges the b-plane coordinate with respect to the no-CAM scenario.

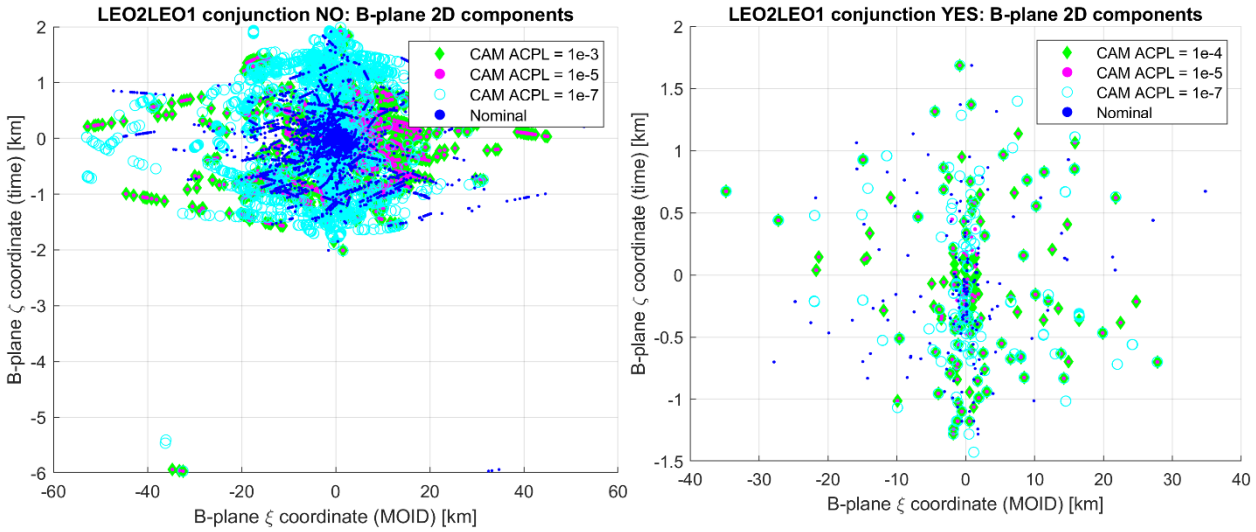

a) B-plane representation. Concept of operations: standard b) B-plane representation. Concept of operations: new

Figure 10: Characterisation of the LEO2LEO CAM scenarios.

6. Conclusion

This paper shows the application of a method for the computation of CAMs: a semi-analytical fuel-optimal method with Chan's PoC boundary condition. This method has been applied to target a predefined ACPL value showing very reliable results.

Large simulations were performed for the fuel optimal approach, and it was shown that in all the scenarios, namely Geostationary orbit station keeping (GEOSK), graveyard orbit (GRAVEYARD), GTO to GEO transfer (GTO2GEO1 and GTO2GEO3), LEO to LEO transfers (LEO2LEO) and LEO large-constellation transfers (LEOMEGCONST), the method is able to achieve a pre-defined ACPL. For each of them two concepts of operations were considered, the

DOI: 10.13009/EUCASS2023-061

STANDARD one (NO) and the new PROPOSED one (YES). In some cases, the lowest value of ACPL 1e-7 was not achieved due to numerical errors when targeting an exact value of the ACPL and to the very short warning time, especially in the new concept of operations approach. A future extension of the method will try to minimise the PoC when an exact ACPL cannot be achieved. Moreover, future works will study the sensitivity analysis in terms of orbital position of the CA and of the CAM to link the results to some orbital mechanics insights.

Acknowledgements

This work has received funding from the European Space Agency through the project "ELECTROCAM: Assessment of collision avoidance manoeuvre planning for low-thrust missions" (call AO/1-10666/21/D/SR).

References

[1] Maestrini, M., De Vittori, A., Di Lizia, P., and Colombo, C. 2022. Dynamics-Based Uncertainty Propagation with Low-Thrust. In: *2022 AAS/AIAA Astrodynamics Specialist Conference*, Charlotte, NC, USA, 7-11 Aug. 2022.

[2] Maestrini, M., De Vittori, A., Gonzalo, J.L., Colombo, C., Di Lizia, P., Míguez Arenas, J., Sanjurjo Rivo, M., Diez Martín, A., Gago Padreny, P., and Escobar Antón, D. 2023. ELECTROCAM: Assessing the Effect of Low-Thrust Uncertainties on Orbit Propagation. In: *2nd ESA NEO and debris detection conference*, Darmstadt, Germany, 24-26 Jan. 2023.

[3] Gonzalo, J.L., Colombo, C., and Di Lizia, P. 2022. Single-averaged models for low-thrust collision avoidance under uncertainties. In: *73rd International Astronautical Congress*, Paris, France, 18-22 Sept. 2022.

[4] Gonzalo, J.L., Colombo, C., and Di Lizia, P. 2020. Introducing MISS, a new tool for collision avoidance analysis and design. *Journal of Space Safety Engineering*, 7(3): 282-289. https://doi.org/10.1016/j.jsse.2020.07.010

[5] Gonzalo, J.L., Colombo, C., and Di Lizia, P. 2021. Computationally efficient approaches for low-thrust collision avoidance activities. In: *72nd International Astronautical Congress*, Dubai, UAE, 25-29 Oct. 2021.

[6] Hernando-Ayuso, J., and Bombardelli, C. 2020. Low-Thrust Collision Avoidance in Circular Orbits. *Journal of Guidance, Control, and Dynamics*. 44(5):983-995. https://doi.org/10.2514/1.G005547

[7] Chan, K. 2020. Comparison of methods for spacecraft collision probability computations.

[8] De Vittori, A., Palermo, M., Di Lizia, P., and Armellin, R. 2022. Low-Thrust Collision Avoidance Maneuver Optimization. *Journal of Guidance, Control, and Dynamics*, 45(10):1815-1829. https://doi.org/10.2514/1.G006630

[9] Bombardelli, C., Baù, G., and Peláez, J. 2011. Asymptotic solution for the two-body problem with constant tangential thrust acceleration. *Celestial Mechanics and Dynamical Astronomy*, 110:239-256. https://doi.org/10.1007/s10569-011-9353-3

[10] Wittig, A., Colombo, C., and Armellin, R. 2017. Long-term density evolution through semi-analytical and differential algebra techniques. *Celestial Mechanics and Dynamical Astronomy*. 128:435-452. https://doi.org/10.1007/s10569-017-9756-x

[11] Kelley, W.G., and Peterson, A.C. 2010. The theory of differential equations: classical and qualitative. Springer Science & Business Media.